

Short Communication

Visible light-induced photochemical fabrication of ultrathin Ag nanoparticles decorated PPy nanosheets and its oxygen reduction activity

Juan Du¹, Shiming Meng^{1,2,*}, Mei Yu¹, Jianhua Liu¹, Songmei Li¹

¹ School of Materials Science and Engineering, Beihang University, Beijing 100191, China

² School of Aeronautic Science and Engineering, Beihang University, Beijing 100191, China

*E-mail: mengshm@buaa.edu.cn

Received: 22 October 2020 / Accepted: 6 January 2021 / Published: 28 February 2021

In this work, Ag nanoparticles decorated Polypyrrole (PPy) nanosheets were synthesized on the surface of Ag₃PO₄ nanoparticles (APNPs) by a visible light-induced photochemical method in a simple pyrrole solution. Independent Ag nanoparticles decorated PPy nanosheets (UAPNs) was obtained after nitric acid dissolution and sonication. The APNPs were used as visible-light photocatalyst, templates and silver source in the preparation process. The morphology, structure and composition of the resulting hybrid materials were characterized by a variety of characterization methods, which demonstrated that the photoreduced Ag nanoparticles were uniformly deposited in the photooxidized PPy nanosheets through this APNPs based visible light-induced photochemical method, forming the microsized UAPNs with a thickness less than 10 nm. The resulting UAPNs show a good electrocatalytic activity for oxygen reduction reaction (ORR) in alkaline solution.

Keywords: Ag nanoparticles; polypyrrole; photochemical; nanosheets; oxygen reduction reaction

1. INTRODUCTION

In recent years, the synthesis and property characterization of two dimensional nanomaterials have attracted extensive attention, especially for ultrathin nanosheets like graphene, due to their unique physical and chemical properties [1]. As an attractive functional conductive polymer, Polypyrrole (PPy) is a promising support for the immobilization of metal nanoparticles to form hybrids with excellent catalysis and sensing performance [2, 3]. Nanoscale PPy based hybrid materials have been fabricated, exhibiting excellent properties [4-6]. However, the studies on ultrathin PPy-metal nanosheets are rare, which is expected to exhibit distinct properties on catalysis and sensing performance [7].

Various fabrication methods have been developed to prepare two-dimensional materials, such as template method [8], wet-chemical synthesis [9] and liquid exfoliation [10]. As an in-situ fabrication method, semiconductor induced photochemical reaction is considered as a good candidate due to the high reaction rate and environmentally friendliness [11]. Ag_3PO_4 as a photocatalyst exhibits extremely high photooxidative capabilities under visible-light irradiation [12]. Moreover, it is confirmed that Ag particles are easily formed on its surface during photocatalytic process [13].

In this paper, an Ag_3PO_4 based visible light-induced photochemical method was developed to produce ultrathin Ag decorated-PPy nanosheets (UAPNs) efficiently in a Pyrrole monomer aqueous solution. The Ag_3PO_4 nanoparticles were used as visible-light photocatalyst, templates and silver source for the fabrication of UAPNs. The electrocatalytic ORR activity of the resulting UAPNs was studied in alkaline solution.

2. EXPERIMENTAL PROCEDURE

2.1. Materials

Pyrrole monomer was procured from Sinopharm Chemical Reagent Co.,Ltd. Na_2HPO_4 , AgNO_3 and Nitric acid were purchased from Tianjin chemical Limited. Pyrrole monomer was purified by vacuum distillation and other chemicals of analytical grade were used without further purification.

2.2. Synthesis process

10ml Na_2HPO_4 aqueous solution (0.15 M) were added to a 90ml transparent silver ammonia solution containing 0.2g AgNO_3 . The resulted olivine Ag_3PO_4 nanoparticles were filtered and washed with deionized water and then dried for 12 hours in a vacuum oven at 60°C .

The synthesized Ag_3PO_4 nanoparticles (0.2 g) was added into a magnetic-stirred Pyrrole solution (50mL, 0.01 M), and then illuminated with visible light using a 300w xenon light source for ten minutes. The product were filtered and washed by using deionized water and ethanol in sequence, and dried overnight in a vacuum oven at 60°C . The solid samples were washed and ultrasonic treated with a 1M HNO_3 solution in order to achieve the UAPNs. After centrifugation and washed with deionized water to neutral, the UAPNs sample was freeze-dried.

2.3. Instrumentations and characterizations

The microstructures and morphologies of the obtained samples were analyzed with scanning electron microscopy (SEM, XL30 S-FEG) and transmission electron microscopy (TEM, JEOL-2100F). All samples' structures were characterized by X-ray powder diffraction (XRD) through an X-ray diffraction (D/MAX-2500) with Cu $K\alpha$ radiation ($\lambda = 1.5418^\circ\text{A}$) at a scanning rate of $6^\circ/\text{min}$. UV-vis absorption spectra were investigated at room temperature by a UV-3600 spectrometer. Fourier transform

infrared spectroscopy (FTIR) were recorded on a Nicolet-20DXB spectrophotometer to elucidate the surface functional groups.

The electrocatalytic activity of the obtained UAPNs toward ORR was measured with a VersaSTAT VMC electrochemical analyzer. For all electrochemical measurement, a typical three-electrode cell was applied with a catalysts preloaded glassy carbon rotating disk electrode, a graphite rod electrode and an Ag/AgCl (saturated KCl) electrode used as the working, counter and reference electrodes, respectively. The resulting UAPNs (3 mg) were ultrasonic predispersed in 1mL ethanol with 40 μ L 5wt% nafion solution for 30 min. In order to prepare the working electrode, 40 μ L of the prepared solution was dropped on the surface of the glassy carbon. Cyclic voltammetry (CV) tests were recorded at a voltage range between -0.2 and 1.2 V (vs. Ag/AgCl electrode) under a scan rate of 50 mV s⁻¹ in O₂-saturated 0.1 M KOH solution. The Linear sweep voltammetry (LSV) curves were measured under a scan rate of 5 mV s⁻¹ in 0.1 M KOH solution with O₂ flow continuously supplied throughout the process within a series of rotation speeds from 100 to 2025 rpm.

3. RESULTS AND DISCUSSION

3.1. Morphology and structure of the UAPNs

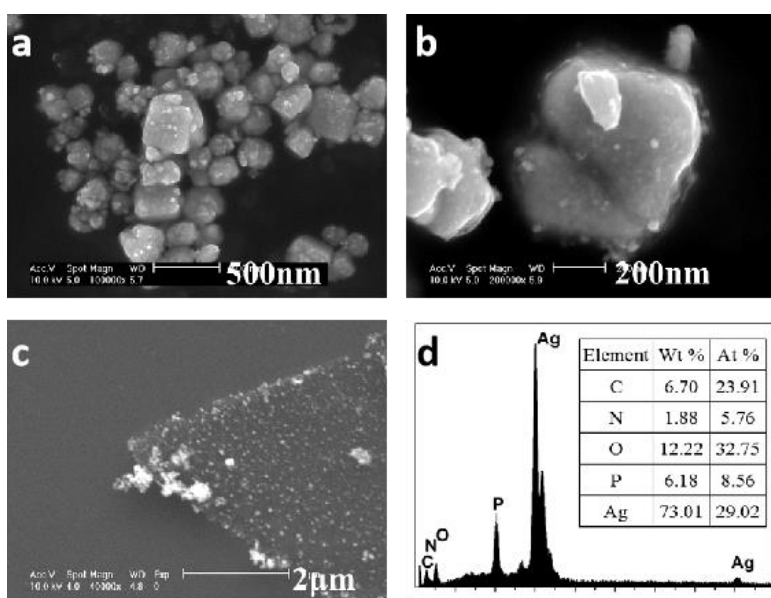


Figure 1. Typical SEM image of PANPs (a and b) and UAPNs (c); (d) EDS of PANPs

Figure 1a and b show the SEM images of the samples synthesized by the photochemical reaction. It can be seen that PPy nanosheets with embedded Ag nanoparticles deposited on the surface of the Ag₃PO₄ nanoparticles, forming the Ag decorated-PPy nanosheet covered Ag₃PO₄ nanoparticles (PANPs) structures. Figure 1c shows the SEM image of the UAPNs after the dissolution of the Ag₃PO₄. The obtained film has a micro-sized ultrathin nanosheet structure much bigger than APNPs, which means it is fully unfolded after ultrasonic treatment. The silver particles, with the particle size of several tens of nanometers, are evenly dispersed on the nanosheets, although with some aggregation at the edges. As

displayed in Figure 1d, the atomic ratio of different elements from the EDS result demonstrates that the silver, PPy and silver phosphate are all present in the PANPs.

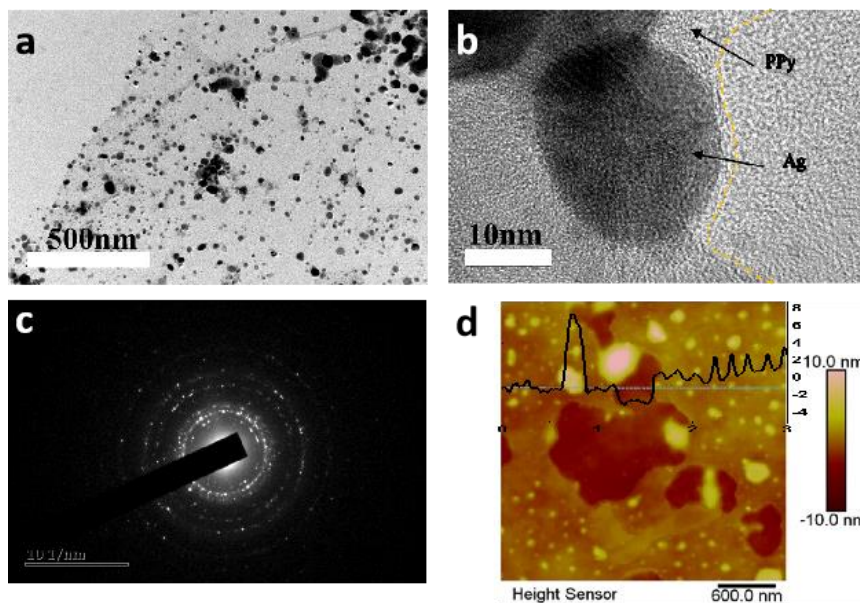


Figure 2. Typical TEM image of (a) (b) UAPNs; (c) SAED pattern of Ag nanoparticles in UAPNs; and (d) AFM image of UAPNs

TEM images in Fig. 2a and b show that uniformly distributed Ag nanoparticles are successfully deposited in the main body of PPy nanosheets, which indicates that photoinduced oxidation of pyrrole and reduction of silver occur simultaneously on the excited surface of APNPs. The particle size of silver nanoparticles presents a discrete distribution, but most of them are about tens of nanometers, besides some excessively grown ones. The electron diffraction pattern in Figure 2c shows that the silver nanoparticles are polycrystalline. As shown in Figure 2d, the thickest part of the UAPNs is less than 10 nm, and the average thickness is around 4nm, which implying the retarding effect of PPy on the growth of silver nanoparticles in the direction perpendicular to the plane of the nanosheet.

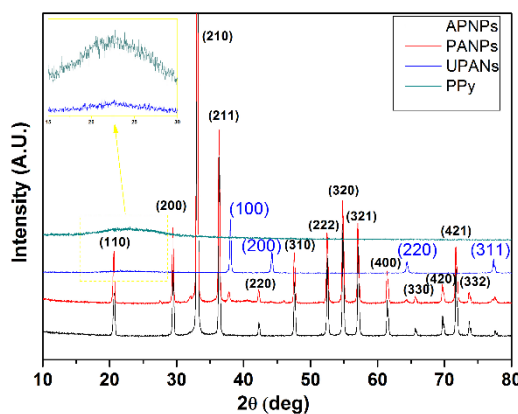


Figure 3. X-ray diffraction patterns of the samples: APNPs, PANPs, UAPNs, PPy

The XRD patterns of the samples are shown in Figure 3. In comparison with the patterns of APNPs and PPy, the PANPs have a significant absorption peak at 36.1° , corresponding to the (111) absorption peak of cubic silver. It indicates the presence of Ag nanoparticles on the surface of APNPs [14]. This peak can also be seen in the pattern of the UAPNs sample. A broad peak at around 25° indicates that the amorphous PPy is also present in the UAPNs.

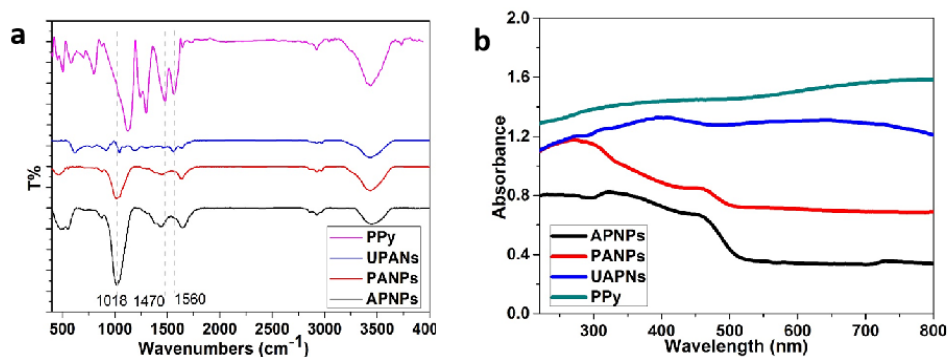


Figure 4. FTIR spectra (a) and UV-Vis spectra (b) of the samples: APNPs, PANPs, UAPNs, PPy

FTIR spectra of the products are shown in Figure 4a. The presence of PPy in UAPNs is confirmed by the characteristic peaks at 1550 cm^{-1} and 1460 cm^{-1} , which assigns to typical pyrrole ring vibrations (C-C and C-N) [15]. The typical peak of Ag_3PO_4 centered at about 1018 cm^{-1} is not observed in the spectrum of UAPNs, indicating the complete dissolution of APNPs [16].

Figure 4b shows the UV-Vis diffuse reflectance spectrums of the samples. It is clear that after the growth of UAPNs on the surfaces of APNPs, the absorption edge of PANPs has been slightly extended to around 560 nm from 540 nm for APNPs, and the absorption intensity in the region of 220-800 nm has been evidently increased. It is worth noting that the peak at around 410nm arises in the spectrum of UAPNs, which is the typical UV absorption peak of silver nanoparticle [17]. Furthermore, the spectrums of UAPNs and PPy have the similar curve. These results clearly reveal the successful in-situ growth of UAPNs on APNPs. It also indicates that this method can be used as an alternative route to enhance the visible-light absorption of Ag_3PO_4 .

3.2. Electrochemical measurement of the UAPNs

Figure 5a shows the the cyclic voltammetry of the UAPNs electrode in the O_2 -saturated 0.1 M KOH solution. It exhibits typical cathodic ORR peaks between the applied potential range from -1.2 to 0.2 V, showing the reduction peak potential at -0.32 V. However, no obvious anodic peak of Ag is emerged due to the low Ag loading. To further investigate the ORR electrocatalytic activity of the UAPNs, the RDE measurement was performed at different rotation speeds from 100 to 2025. As clearly shown in Fig.5b, the UAPNs electrode shows the onset potential nearly -0.12V with continually increasing excitation current, which indicates that UAPNs has a high ORR activity. In addition, the

polarization curves reveal typical gradually enlarging current with increased rotating speeds due to the accelerated oxygen flux to the electrode surface caused by the promoted rotating rates[18]. Figure 5c shows the Koutecky-Levich (K-L) plots at the five different potentials for UAPNs. All the plots in the figure exhibit good linearity. The average value of electron transfer numbers (n) for UAPNs calculated from the K-L equation are 3.76. This electron transfer number confirms that the ORR of UAPNs proceeds the co-existence of two and four-electron pathways, while the four-electron pathway was a major pathway[19]. The above results indicated that the thin 2D structure of UAPNs with dispersed Ag nanopaticals is favourable to enhance the ORR by providing fast ions and electrons transport and abundant reactive sites. The comparison on the ORR performance of UAPNs and other similar catalysts have been provided in Table 1 , which reveal the good catalytic performance of the prepared UAPNs. In general, the prepared UAPNs by this photochemical strategy can be regarded as a possible composite catalyst for ORR.

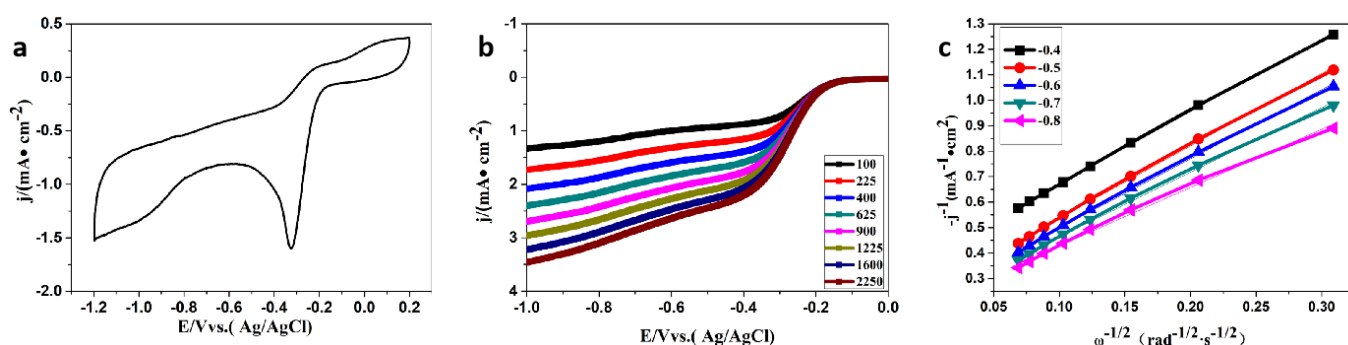


Figure 5. Electrochemical measurements of the UAPNs electrode in O_2 -saturated 0.1 M KOH. (a) CV curves, (b) RDE voltammograms for ORR at different rotation speeds, (c) K-L plots (i^{-1} vs. $\omega^{-1/2}$) at different potential.

Table 1. Comparison of ORR performance over similar catalysts.

Materials	ORR peak vs Ag/AgCl	The onset potential	n values	solution	Ref.
silver nanoclusters	–	–0.13V	2.8	O_2 -saturated 0.1 M KOH	[20]
silver nanoparticles/ N-doped carbons	–0.28 V	–0.174 V	3.41	O_2 -saturated 0.1 M KOH	[21]
thin-film Ag	–	–0.2V	3.8	O_2 -saturated 0.1 M KOH	[22]
MPS-nano Ag/NF film	–0.4 V	–	–	PBS solution (pH 7.4)	[23]
LbL films of ATP-Ag NPs	–0.4 V	–0.1 V	3.2	O_2 -saturated 0.1 M NaOH	[24]
Ag-PVP/GC	–0.4 V	–	3.8	O_2 -saturated 0.1 M KOH	[25]
UAPNs	–0.32 V	–0.12V	3.76	O_2 -saturated 0.1 M KOH	This work

4. CONCLUSIONS

In summary, ultrathin Ag nanoparticles decorated-PPy nanosheets have been fabricated via the in situ photoinduced polymerization of pyrrole and the reduction of Ag^+ on the surface of APNPs. The thickness of the obtained UAPNs is less than 10nm. The polycrystalline Ag nanoparticles are uniformly dispersed in the polypyrrole nanosheets, although with discrete size distribution. The resulting UAPNs show potential applications as ORR electrocatalyst in alkaline solution. Furthermore, this preparation strategy may also be adapted for preparing other conductive polymer/metal nanoparticles heterostructures rather than nanosheets.

ACKNOWLEDGEMENTS

This work was supported by the fundamental research funds for central universities (YWF-19-BJ-J-210; YWF-20-BJ-J-546)..

References

1. W.L. Yang, X.D. Zhang, Y. Xie, *Nano Today*, 11 (2016) 793.
2. Q.Q. Zhou, G.Q. Shi, *J. Am. Chem. Soc.*, 138,(2016) 2868.
3. Y. Liu, Z. Liu, N. Lu, E. Preiss, S. Poyraz, M.J. Kim, X. Zhang, *Chem. Commun.*, 48(2012) 2621.
4. A.J. Suryawanshi, P. Thuptimdang, J. Byrom, E. Khan, V.J. Gelling, *Synth. Met.*, 197 (2014) 134
5. L.Y. Yuan, C.Y. Wan, X.R. Ye, F.H. Wu, *Electrochim. Acta*, 213 (2016) 115
6. X.M. Yang, Y. Lu, *Mater. Lett.*,59 (2005) 2484.
7. S.S. Jeon, H.H. An, C.S. Yoon, S.S. Im, *Polymer*, 52(2011) 652.
8. D.K. Hwang, D. Song, S.S. Jeon, T.H. Han, Y.S. Kang, S.S. Im, *J. Mater. Chem. A.*, 2(2014) 859
9. C. Tan, H. Zhang, *Nat. Commun.*, 6 (2015) 7873
10. C. Backes, T.M. Higgins, A. Kelly, C. Boland, A. Harvey, D. Hanlon, J.N. Coleman, *Chem. Mat.* 29(1) (2017) 243
11. G. Menagen, J.E. Macdonald, Y. Shemesh, I. Popov, U. Banin, *J. Am. Chem. Soc.*, 131 (2009) 17406
12. Z.G. Yi, J.H. Ye, N. Kikugawa, T. Kako, S.X. Ouyang, H. Stuart-Williams, H. Yang, J.Y. Cao, W.J. Luo, Z.S. Li, Y. Liu, R.L. Withers, *Nat. Mater.*, 9(2010) 559.
13. W. Zhou, W.H. Liu, S.Q. Hu, *Int. J. Electrochem. Sci.*, 15(2020) 4546.
14. G.A. Martinez-Castanon, N. Nino-Martinez, J.P. Loyola-Rodriguez, N. Patino-Marin, J.R. Martinez-Mendoza, F. Ruiz, *Mater. Lett.*, 63(15) (2009) 1266
15. H. Zhou, G. Han, Y. Xiao, Y. Chang, H.-J. Zhai, *J. Power Sources*, 263 (2014) 259
16. M. Thomas, S.K. Ghosh, K.C. George, *Mater. Lett.*, 56(4) (2002) 386
17. K.G. Stamplecoskie, N.L. Pacioni, D. Larson, J.C. Scaiano, *J. Am. Chem. Soc.*, 133 (2011) 9160.
18. T.T. Yang, M. Wang, X.P. Ju, J.S. Zhao, C.G. Fu, *Int. J. Electrochem. Sci.*, 12 (2017) 12125.
19. G. Nam, J. Park, S. T. Kim, D. B. Shin, N. Park, Y. Kim, J. S. Lee and J. Cho, *Nano. Lett.*, 14 (2014) 1870.
20. Y.Z. Lu, W. Chen, *J. Power Sources*, 197 (2012) 107.
21. G.Panomswan, J. Chantaramethakul, C. Chokradjaroen, T. Ishizaki, *Mater. Lett.*, 251 (2019) 135.
22. J.M. Linge, H. Erikson, A. Kasikov, M. Rähn, V. Sammelseg, K. Tammeveski, *Electrochim. Acta*, 325 (2019) 134922.
23. H.W. Cheng, S. Thiagarajan, S.M. Chen, *Int. J. Electrochem. Sci.*, 6 (2011) 4150.
24. P. Singh, D.A. Buttry, *J. Mater. Chem. C*, 116 (2012) 10656.

25. Y.Z. Lu, Y.C. Wang, W. Chen, *J. Power Sources*, 196 (2011) 3033.

© 2021 The Authors. Published by ESG (www.electrochemsci.org). This article is an open access article distributed under the terms and conditions of the Creative Commons Attribution license (<http://creativecommons.org/licenses/by/4.0/>).